EPR, charge transport, and spin dynamics in doped polyanilines

A. L. Kon'kin, V. G. Shtyrlin,* R. R. Garipov, A. V. Aganov, and A. V. Zakharov
Kazan State University, 18 Kremlevskaya, Kazan 420008, Russian Federation

V. I. Krinichnyi
Institute of Problems of Chemical Physics, Russian Academy of Sciences, Chernogolovka, 142432 Moscow Region, Russian Federation

P. N. Adams and A. P. Monkman
Department of Physics, University of Durham, South Road, Durham, England
(Received 31 January 2002; published 6 August 2002)

Charge transport and magnetic properties of films of polyaniline (PAN) doped with 10-camphorsulfonic acid and 2-acrylamido-2-methyl-1-propanesulfonic acid (AMPSA) have been studied by conductivity, magnetic-susceptibility superconducting quantum interference device measurements, and 3-cm and 8-mm electron paramagnetic resonance (EPR) spectroscopy at doping levels (x) from 0.3 to 0.9 over a temperature range from 15 to 300 K. The temperature dependences of conductivities were explained in terms of the advanced multiphase heterogeneous granular metallic (HGM) model with percolation including disordered metallic (DM) and nonmetallic (NM) phases. The anomalous conductivity change in the PAN-AMPSA$_x$ system at $T>240$ K was accounted quantitatively for a solid-phase equilibrium with the occurrence of the disordered anion phase from the metallic islands. A means for analysis of the EPR line shape in conducting media has been developed and, with this, conductivity and microwave dielectric constants were estimated and two EPR signals, R_1 and R_2, were detected in both systems. It was shown that R_1 signal belongs to pinned radicals of isolated polymer chains, whereas R_2 is the weight-averaged signal, resulting from three types of paramagnetic centers, localized and mobile spins in the NM and DM phases, which interact via exchange. From the temperature and frequency dependences of the R_2 linewidth the spin-diffusion parameters for the NM phase in both systems were determined. It was found that the HGM model allows good explanation of both charge transport and spin diffusion in the doped polyaniline films.

DOI: 10.1103/PhysRevB.66.075203 PACS number(s): 73.50.−h, 75.70.Ak, 76.30.−v, 72.80.Le

I. INTRODUCTION

Conducting polymers based on polyaniline (PAN) have attracted much attention owing to their stability under environmental conditions and diversified and unusual properties (see, e.g., Ref. 1). The highly conducting emeraldine salt of polyaniline (PAN-ES) is formed by protonation of the semiconducting emeraldine base (PAN-EB), see Fig. 1, without addition or removal of electrons. Depending on protonation (doping) level, acid nature, preparation conditions, and subsequent treatments, conductivities (σ) of the doped PAN materials exhibit nonmetallic behavior ($d\sigma/dT>0$) in some temperature (T) ranges, sometimes with a change to metallic sign ($d\sigma/dT<0$) at high temperatures, or crossover through an insulator-metal transition.[2,3]

A quasi-one-dimensional (quasi-1D) morphology, disorder, and microheterogeneity play key roles in the charge delocalization of these systems.[4–15] However, there are many controversies concerning the nature of the intrinsic charge-transfer processes on the microscopic or mesoscopic scales. One issue is whether the electronic localization is caused by homogeneous disorder [one dimensional[16] (1D) or three dimensional[17] (3D)] or inhomogeneous disorder.[10,12–14] Another controversy is whether the temperature dependence of σ in nonmetallic region ($d\sigma/dT>0$) is indicative of quasi-1D variable range hopping[2,3,5,14,18–20] (VRH), phonon-assisted hopping[10,14,16,21,22] or 3D charge tunneling between metallic islands [granular metallic model (GMM)].[4,8,9,14,23–25] A central problem is still the nature of the intrinsic metallic state and the temperature dependence of σ in metallic regime. As a consequence, a universal description of the conducting polymer's transport properties over the full temperature and composition ranges has not been achieved up to the present. The conductivity vs temperature dependences, with a maximum revealing the metallic state, have been depicted previously for some highly doped PAN materials[26–29] in terms of heterogeneous model with contribution from fluctuation-induced tunneling,[30] however, the re-

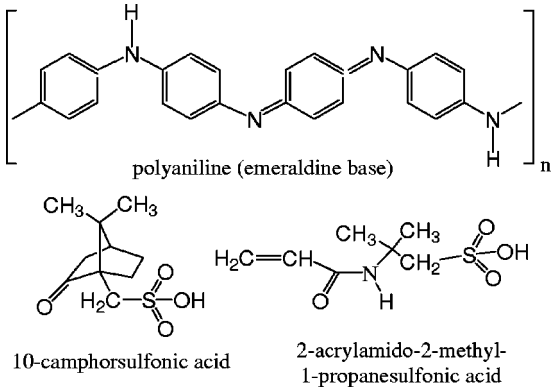

FIG. 1. Chemical structures of the polyaniline (emeraldine base) (PAN-EB), and the acid dopants, 10-camphorsulfonic acid (CSA) and 2-acrylamido-2-methyl-1-propanesulfonic acid (AMPSA), used in this study.

lationships between the fitting parameters obtained and polymer compositions were not analyzed. In the present work an effort will be made to reach the general and physically clear description of conductivities in two doped PAN systems throughout the investigated ranges of temperatures and doping levels.

The macroscopic conductivity of the polymers may arise from several intrinsic charge-transfer processes on the microscopic or mesoscopic scales. Since doped PAN systems possess unpaired electrons, with spin $S=1/2$, the electron paramagnetic resonance (EPR) method may be very useful for studying such processes. The advantages of the method are the possibility to record several paramagnetic centers, to measure their paramagnetic susceptibilities (χ), and to determine the anisotropic coefficients of spin diffusion along a 1D polymer chain ($D_{\|}$) and between chains ($D_{\perp}$). Further, as we shall demonstrate below, the EPR method enables one to estimate conductivity and microwave dielectric constant ($\varepsilon_{\mathrm{MW}}$) in a metallic state of polymers.

The previous EPR investigations of the doped PAN systems have given contradictory and puzzling results.[5,14,19,20,31–40] In all instances one EPR signal was detected with spin susceptibility involving a temperature-independent Pauli-like contribution (χ_{P}) and a temperature-dependent Curie-like contribution (χ_{C}). The temperature and/or frequency dependences of the EPR linewidth obtained in different works cited above are drastically dissimilar and sometimes unusual. The $D_{\|}$ and $D_{\perp}$ coefficients estimated from EPR data[19,36–38] or EPR and nuclear magnetic resonance data[35] were explained by authors[19,35–38] in terms of quasi-1D spin diffusion without regard for heterogeneity and possible 3D nature of metallic state in the polymers. Many of the discrepancies in the EPR results may originate from incorrect fitting of the EPR line shape. Because of this, we shall give a method of a complete analysis of the EPR lines in the metallic state of the polymers.

In this paper, we present the results of a charge transport and magnetic study of polyaniline films prepared as highly doped with 10-camphorsulfonic acid (CSA) and 2-acrylamido-2-methyl-1-propanesulfonic acid (AMPSA), see Fig. 1, by conductivity, magnetic-susceptibility superconducting quantum interference device (SQUID) measurements, and 3-cm and 8-mm EPR spectroscopy over a temperature range from 15 to 300 K. By application of the method of EPR line shape analysis that we have developed, two Dysonian-like EPR signals, R_1 and R_2, were originally detected and assigned to pinned and mobile paramagnetic centers, respectively. All of the multitude of the temperature dependences of the quantities σ, χ, and EPR linewidth (ΔH) at different doping levels (x) in the PAN-CSA_x and PAN-AMPSA_x systems is unambiguously explained in terms of a heterogeneous effective-medium model with percolation including disordered metallic (DM) and nonmetallic (NM) phases. These phases each incorporate the crystalline metallic islands with an amorphous shell but in the DM phase the barrier widths between islands are so narrow that they provide the 3D charge delocalization. It is shown that localized and mobile spins interact via exchange to yield the weight-averaged EPR signal R_2, whereas R_1 belongs to radicals of isolated polymer chains. Based on this model we compute fractions and charge-transfer and spin-diffusion parameters for DM and NM phases. When compared to PAN-CSA_x, the PAN-AMPSA_x system reveals an anomalous behavior at $T>240$ K, which is accounted quantitatively for a solid-phase equilibrium with the metallic islands disordering through a thermally increased motion of the AMPSA counteranions hydrogen bonded to the PAN backbone. Within the framework of our model the charge-transfer and spin-diffusion mechanisms in conducting polymers are analyzed.

In this paper a conceptual model is introduced initially for the interpretation of the conductivity data and supported and evolved as the EPR and magnetic-susceptibility parameters were examined.

II. EXPERIMENTAL METHODS

As a starting material, high-molecular-weight PAN-EB, synthesized in Durham by the outlined procedure,[41] has been used. The doping levels $x=[\text{acid}]/[\text{nitrogen site}]$, ranging between 0.3 and 0.9 were achieved by the stoichiometric addition of acid (CSA or AMPSA) to the polymer using *m*-cresol or dichloroacetic acid as solvents.[28,29] The dark green solutions were poured onto silicon wafers and dried in air at 40 °C, yielding films typically 50-μm thick. The direct current (dc) conductivities of the films were measured between 15 and 300 K, using standard four-in-line evaporated gold electrode geometry.

EPR measurements were performed using X-band (9.3 GHz, 3 cm) ''Thomson'' and K-band (36.7 GHz, 8 mm) EPR spectrometers with a 30- or 100-kHz magnetic-field modulation for a phase-lock detection. EPR spectra were recorded in the 14–300 K temperature range (except for K band) with an Oxford ESR cryostat. The simulation of the EPR spectra was performed by application of the methodology outlined below. The static magnetic-susceptibility measurements as a function of temperature were made using a SQUID magnetometer in Laboratory of Novel Materials of Kazan Physical-Technical Institute RAS. All calculations have been carried out using an in-house ORIGIN 5.0 program.

III. RESULTS AND DISCUSSION

A. dc conductivity and charge transport mechanism

The temperature dependences of the dc conductivity, $\sigma_{\mathrm{dc}}(T)$, for the PAN-CSA_x and PAN-AMPSA_x samples are shown in Figs. 2 and 3. The PAN-CSA_x system will be dealt with first.

At low doping level, $x=0.3$, the $\sigma_{\mathrm{dc}}(T)$ dependence for the PAN-CSA_x sample is distinguished by a nonmetallic (NM) slope of the curve ($d\sigma/dT>0$) and adequately described by the equation

$$\sigma_{\mathrm{NM}}=\sigma_0\exp[-(T_0/T)^{\gamma}] \tag{1}$$

with $\gamma=1/2$. More than one model predicts a $\sigma_{\mathrm{dc}}(T)$ dependence following Eq. (1) with $\gamma=1/2$: (i) Mott's VRH model that calls for $\gamma=1/(1+d)$, where d is system's dimensionality, and so $\gamma=1/2$ for quasi-1D transport;[2,3] (ii) Efros-Shklovsky model,[42,43] which predicts $T^{-1/2}$ law for 3D VRH

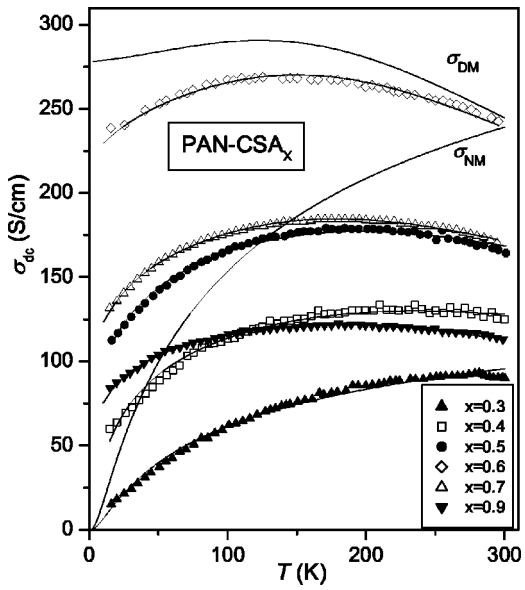

FIG. 2. The temperature dependences of the experimental dc conductivity σ_{dc} (points) and calculated σ_{eff}, σ_{NM} and σ_{DM} conductivities (lines) in the PAN-CSA$_x$ system at different doping levels x.

in the presence of a Couloumb gap in the density of states near Fermi level; (iii) based on the GMM approach[23,24] models of 3D hopping between the metallic islands correspond to single strands[8] or mesoscopic crystalline regions;[9,25] and (iv) the model of correlated 3D hopping between polaronic clusters (not necessary metallic).[44] In the case of doped PAN, there are many arguments in favor of the GMM model, (iii) (see Refs. 8 and 9). One of the important arguments is evident from data in Fig. 2. Actually, the high-temperature metallic behavior of σ_{dc} at doping levels $x=0.4$–0.9 suggests

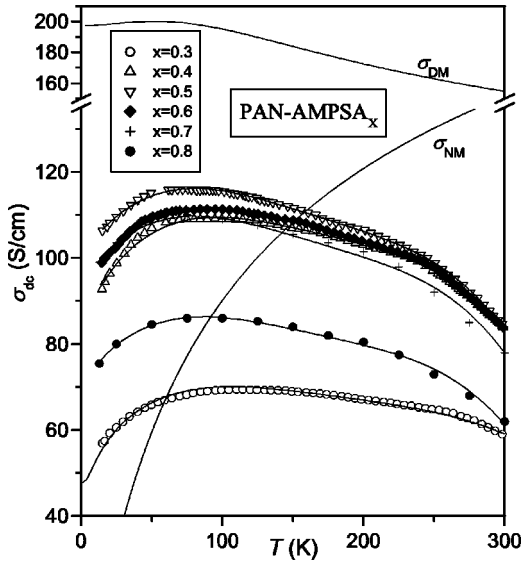

FIG. 3. The temperature dependences of the experimental dc conductivity σ_{dc} (points) and calculated σ_{eff}, σ_{NM} and σ_{DM} conductivities (lines) in the PAN-AMPSA$_x$ system at different doping levels x.

the presence of metallic islands (clusters) just near the percolation threshold $x_c=0.3$–0.4. As the T_0 parameter is proportional to the separation between neighboring metal grains, s,[8,9,23,24] the T_0 value for $x=0.3$ closely corresponds to the critical s magnitude from which a 3D network of the metallic state is formed.

Above the percolation threshold the NM and DM phases can coexist. For the description of the DM phase conductivity (σ_{DM}), the universal $\sigma(T)$ dependence for disordered metals appeared as the most suited model put forward by Kaveh and Mott[45] and developed from previous ideas (see Refs. 46 and 47):

$$\sigma_{DM}=\sigma_B\left[1-\frac{3}{(k_F l_0)^2}\left(1-\frac{l_0}{L_{in}}\right)\right], \tag{2}$$

where

$$\sigma_B=\frac{1}{3\pi^2}\frac{e^2}{\hbar}k_F^2\left(\frac{1}{l_0}+\frac{1}{l_{in}}\right)^{-1} \tag{3}$$

and

$$L_{in}=\left(\frac{1}{2}l_0 l_{in}\right)^{1/2}. \tag{4}$$

In relations (2)–(4), k_F is the wave vector at the Fermi level, l_0 and l_{in} are the elastic and inelastic electron mean free paths, respectively, and L_{in} is the maximum length of electron diffusion without being interrupted by an external perturbation. Introducing the mean time between inelastic electron-phonon collisions, $\tau_{in}(T)=l_{in}(T)/v_F$, and the scattering time due to static disorder, $\tau_0=l_0/v_F$ (where v_F is the Fermi velocity), relation (2) may be rewritten as

$$\sigma_{DM}=a\frac{\tau_0\tau_{in}}{\tau_0+\tau_{in}}\left[1-b\left(1-\frac{(2\tau_0)^{1/2}}{(\tau_{in})^{1/2}}\right)\right], \tag{5}$$

where

$$a=\frac{1}{3\pi^2}\frac{e^2}{\hbar}k_F^2 v_F \quad \text{and} \quad b=\frac{3}{(k_F l_0)^2}.$$

The temperature dependence of σ_{DM} originates from the temperature dependence of l_{in} (τ_{in}). The Eqs. (2)–(5) predict a change of the $d\sigma/dT$ sign from positive to negative with increasing temperature (decreasing l_{in} and τ_{in}) for the sufficiently large $k_F l_0$ values (>1). Notice that the positive $d\sigma/dT$ may be ascribed to the power-law Anderson "localization" effects.[48] For the electron-phonon scattering, it is generally believed that $\tau_{in}\propto T^{-3}$ at $T<\theta_D$ and $\tau_{in}\propto T^{-1}$ at $T>\theta_D$, where θ_D is the Debye temperature. We introduce the following empirical function describing such behavior of τ_{in}:

$$\tau_{in}=\frac{c}{T^3}+\frac{d}{T^2}\frac{1}{\exp(\theta_D/T)-1}, \tag{6}$$

where c, d, and θ_D are fitting parameters.

TABLE I. Parameters of the heterogeneous granular metallic (HGM) model calculated by Eqs. (1) and (5)–(7) for the PAN-CSA_x system at different doping levels x. $\sigma_0=438$ S/cm, $T_0=110$ K, $a=3.03\times10^{16}$ S/(cm s), $b=0.234$, $\tau_0=1.20\times10^{-14}$ s, $c=5.06\times10^{-7}$ sK^3, $d=3.12\times10^{-10}$ sK^2, and $\theta_D=130$ K.

x	c_{NM}	c_{DM}	c_{NC}
0.3	0.600	0	0.400
0.4	0.323	0.363	0.314
0.5	0.259	0.537	0.204
0.6	0.088	0.872	0.014
0.7	0.198	0.605	0.197
0.9	0.152	0.491	0.357

Considering the PAN-CSA_x system as an inhomogeneous material with three phases, NM PAN-ES, DM PAN-ES, and practically nonconducting (NC) phase (PAN-EB or excess of dopant), the bulk conductivity of this system (σ_{eff}) may be well described within the framework of the effective-medium theory by equation[49]

$$\sum_i c_i \frac{\sigma_i-\sigma_{eff}}{2\sigma_{eff}+\sigma_i}=0, \tag{7}$$

where c_i is the volume fraction of the ith component (phase) and σ_i is its conductivity. In this instance we have $\sigma_1=\sigma_{NM}$, $\sigma_2=\sigma_{DM}$, and $\sigma_3=\sigma_{NC}=0$.

The results of computations of the heterogeneous model parameters for the PAN-CSA_x system by Eqs. (1) and (5)–(7) are given in Table I. The calculated $\sigma_{eff}(T)$, $\sigma_{NM}(T)$, and $\sigma_{DM}(T)$ dependences are shown in Fig. 2 as lines. Good fits over the measured temperature range are obtained for all the PAN-CSA_x samples. We emphasize that the calculated volume fraction of the DM phase for PAN-$CSA_{0.5}$ ($c_{DM}=0.531$) is close to the percent of crystallinity, κ, estimated by X-ray structure studies for PAN-$CSA_{0.5}$ ($\kappa=0.36$) (Refs. 50 and 51) and PAN-$HCl_{0.5}$ samples ($\kappa\sim0.5$).[14] It is significant that in the present work the full description of the PAN-CSA_x system conductivity has been achieved with a unified set of model parameters (Table I), contrary to previous simulations[27–29] where fitting parameters varied from one sample to another with x.

We come next to the consideration of the PAN-$AMPSA_x$ system. As is evident from a comparison of the conductivity data in Figs. 2 and 3, the PAN-$AMPSA_x$ differs from the PAN-CSA_x system in that it has a lesser value of the NM-DM percolation threshold, $x_c<0.3$, and the presence of a transition point at 240–260 K, above which the negative $d\sigma/dT$ coefficient becomes much larger in magnitude. Previously[29] in the PAN-$AMPSA_x$ films an endothermic transition centered at 240–254 K with magnitude dependent upon the AMPSA content has been detected by differential scanning calorimetry. There are reasons[29] to assume that this phase transition corresponds to a solid-phase equilibrium between the metallic islands with the ordered AMPSA anions in the side chains and the clusters with the disordered anions (DA phase). Since the metallic islands are present in both DM and prepercolation NM phases with only minor difference in intergrain separation for these phases, the above equilibrium constant (K_D) can be written as

TABLE II. Parameters of the HGM model calculated by Eqs. (1) and (5)–(9) for the PAN-$AMPSA_x$ system at different doping levels x. $\sigma_0=245$ S/cm, $T_0=100$ K, $a=1.93\times10^{16}$ S/(cm s), $b=0.148$, $\tau_0=1.15\times10^{-14}$ s, $c=1.14\times10^{-7}$ sK^3, $d=1.08\times10^{-9}$ sK^2, $\theta_D=140$ K, $\Delta H_D=21.6$ kJ/mol, $\Delta S_D=53$ J/(K mol) [$x=0.4$–0.8], and $\Delta S_D=44$ J/(K mol) [$x=0.3$].

x	c_{NM}	c_{DM}	c_{NC}
0.3	0.152	0.495	0.389
0.4	0.130	0.627	0.243
0.5	0.082	0.678	0.240
0.6	0.108	0.648	0.244
0.7	0.077	0.659	0.264
0.8	0.080	0.576	0.344

$$K_D=\frac{c_{DA}}{c_{NM}+c_{DM}}, \tag{8}$$

with temperature dependence,

$$K_D=\exp(\Delta S_D/R)\exp(-\Delta H_D/RT), \tag{9}$$

where c_{DA} is the volume fraction of the DA phase, ΔS_D and ΔH_D are entropy and enthalpy of the equilibrium, respectively. Hence the fourth component (DA phase) contributes to the conductivity of the PAN-$AMPSA_x$ system according to Eq. (7) and, in view of expression (8), we have $c_{NM}=c_1=[1/(1+K_D)]c_1^0$, $c_{DM}=c_2=[1/(1+K_D)]c_2^0$, and $c_{DA}=c_4=[K_D/(1+K_D)](c_1^0+c_2^0)$, where c_1^0 and c_2^0 are, respectively, the NM and DM phase fractions at low temperatures ($T\to0$). As has already been intimated,[29] the increased AMPSA anions motion in the side chains gives rise to increased movement in the PAN backbone and so to greater phonon backscattering of charge carriers. To a first approximation, the conductivity of the DA phase may be taken as negligibly small, $\sigma_4=\sigma_{DA}=0$, similar to $\sigma_3=\sigma_{NC}=0$. With this assumption the heterogeneous model parameters for the PAN-$AMPSA_x$ system were calculated by relations (1) and (5)–(9). The results are presented in Table II. As Fig. 3 suggests, the agreement between calculated and experimental $\sigma_{dc}(T)$ dependences is excellent.

We point out that the conductivity of the PAN-$AMPSA_x$ system in the full temperature range up to 300 K was fitted here with a unified set of the parameters for all x values (Table II). The high positive entropy values obtained, $\Delta S_D=53$ J/(K mol) for $x=0.4$–0.8 and $\Delta S_D=44$ J/(K mol) for $x=0.3$, is testimony to the disordering of the AMPSA anions, hydrogen bonded to the PAN backbone, at the DA phase formation. As is obvious from the comparison of the data in Tables I and II, the reduced σ_{dc} values for the PAN-$AMPSA_x$ relative to PAN-CSA_x films in the metallic regime ($x\geqslant0.4$) result from the decreasing conductivity both of the NM phase (lower σ_0 magnitude) and DM phase (lower a magnitude). The fractions of the NM and DM phases at the same doping level in both of these systems are

closely related, except the PAN-$CSA_{0.6}$ sample with increased $c_{DM}=0.86$. From the obtained a, b, and τ_0 values, bearing in mind Eq. (5), the Fermi velocity v_F can be estimated by the relation: $v_F=(1/\pi^2)(e^2/\hbar)(1/ab\tau_0^2)$. The v_F values so calculated are 2.4×10^7 and 6.0×10^7 cm/s for the PAN-CSA_x and PAN-$AMPSA_x$ systems, respectively, and close to those evaluated for the PAN-$CSA_{0.5}$ films from the EPR magnetic-susceptibility data [$v_F=(2.8\pm0.8)\times10^7$ cm/s[50] or $(4\pm1)\times10^7$ cm/s[51]].

Apart from the discussed Kaveh-Mott model[45] other more sophisticated theories[52–55] with similar ideas of electron-phonon dynamics were proposed to account for (slope) sign changes of the temperature dependences of the conductivity in disordered metals. However, the conductivity description obtained by use of the universal $\sigma(T)$ dependence[45] in the framework of the advanced multiphase heterogeneous granular metallic (HGM) model should be recognized as quite sufficient and physically clear.

B. EPR line shape, conductivity, and microwave dielectric constant in conducting media

In view of the presence of a metallic state in the PAN-CSA_x and PAN-$AMPSA_x$ systems, there is a need to develop a method for the analysis of the EPR line shape in conductive media. Previously[56] a complete equation for the power absorption in conductive media with a skin depth has been derived. It includes the phase shift due to diffusion of the excited spin, dielectric relaxation of the medium and thickness of the sample and results from simultaneous solution of the Maxwell equations and modified Bloch equations including diffusion:

$$\frac{\partial \mathbf{M}}{\partial t}=\gamma(\mathbf{H}_0\times\mathbf{M}+\mathbf{H}_m\times\mathbf{M})+D\nabla^2\mathbf{M}-\frac{\mathbf{M}}{T_2}, \qquad (10)$$

with $\mathbf{M}$ being the magnetization, $\gamma=g\beta_e/\hbar$, the gyromagnetic ratio, $\mathbf{H}_0$ the temporally constant magnetic field, $\mathbf{H}_m(t)$ the microwave field perpendicular to $\mathbf{H}_0$, D the diffusion coefficient, and T_2 the spin-spin relaxation time. We shall examine the special solution of the equation at $D\to0$ (in more exact terms $T_2\ll T_D$, T_D is the time taken by the excited spin to cross the skin depth[56]) for EPR on localized spins in conducting media. For this special case, it has been demonstrated[57] that the experimentally observed signals of the absorption (χ_A) and dispersion (χ_B) are the linear combinations of both a real part (χ') and an imaginary part (χ'') of the complex high-frequency magnetic susceptibility ($\chi=\chi'-i\chi''$):

$$\chi_A=P\chi'+Q\chi'', \qquad (11a)$$

$$\chi_B=Q\chi'-P\chi'', \qquad (11b)$$

where P and Q are some functions of the size and shape of the sample, conductivity (σ_{dc}), high-frequency microwave (MW) dielectric constant (ε_{MW}), and frequency (ω) of oscillating magnetic field with an amplitude H_{m0}. The Eqs. (11a) and (11b) yield Dysonian line shapes[58] as a special case at $P=Q=1$. With the aim of a more detailed discussion of the experimental data, we represent the calculated results from Altshuler *et al.*[57] in a more expanded form. To do this requires solving the problem of the propagation of a plane electromagnetic wave in a solid medium and to obtain an analytical expression for the flux of the complex Poynting vector. The real and imaginary parts of this flux per unit volume correspond to the paramagnetic absorption (χ_A) and dispersion (χ_B), respectively. The most simple variant for both theory and experiment is a flat plate placed in oscillating magnetic field (Fig. 4). This situation is completely appropriate to the conditions of the EPR signal observation in a right-angled shf resonator (H_{10n} mode).

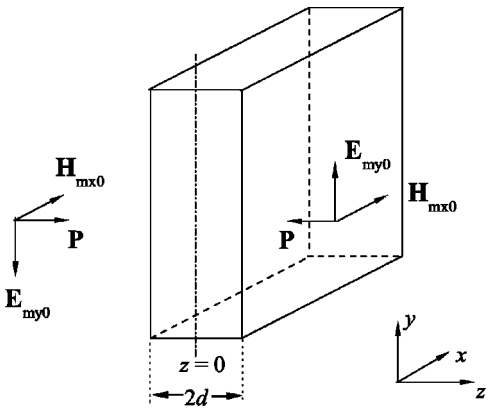

FIG. 4. The relative positions of plane electromagnetic wave and flat plate in the right-angled superhyperfine (shf) resonator.

The initial Maxwell equations in complex form, representing the direction of the wave propagation in the sample (Fig. 4) are

$$\frac{\partial H_{mx}}{\partial z}=(\sigma+\omega\varepsilon)E_{my}$$

and

$$\frac{\partial E_{my}}{\partial z}=-i\omega\mu H_{mx} \qquad (12)$$

(in this and following equations, indices in the σ_{dc} and ε_{MW} symbols are omitted). They give for the H_{mx} component,

$$\frac{\partial^2 H_{mx}}{\partial^2 z}-k^2E_{mx}=0, \qquad (13)$$

with $k^2=-i\omega\mu(\sigma+i\omega\varepsilon)$. The solution of Eq. (13) for the forward and reverse waves with the boundary conditions of $H_{mx}=H_{mx0}$ at the plate surface ($z=\pm d$) may be written as

$$H_{mx}=C_1\exp(-kz)+C_2\exp(kz),$$

where $C_1=C_2=[H_{mx0}/2\cosh(kd)]$. Then the flux Π of the complex Poynting vector, $\mathbf{P}=(\mathbf{E}\times\mathbf{H})$ through unit surface area is given by

$$\Pi=\frac{i\omega\mu}{k}H_{mx0}^2\tanh(kd). \qquad (14)$$

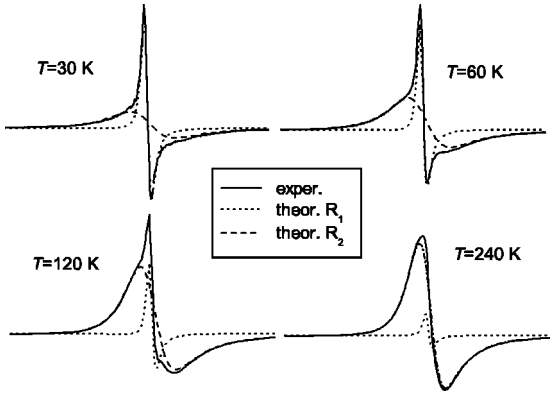

FIG. 5. The experimental and simulated *X*-band EPR spectra of the PAN-$CSA_{0.6}$ film at several temperatures.

As is shown in the Appendix, Eq. (14) can be approximated by the relation

$$\Pi \propto (P\chi' + Q\chi'') + i(Q\chi' - P\chi'') \tag{15}$$

with

$$P = \frac{1}{p^2+q^2}\frac{q\sinh(p) - p\sin(q)}{\cosh(p)+\cos(q)} + \frac{\sin(q)\sinh(p)}{[\cosh(p)+\cos(q)]^2},$$

$$Q = \frac{1}{p^2+q^2}\frac{p\sinh(p) + q\sin(q)}{\cosh(p)+\cos(q)} + \frac{\cos(q)\cosh(p)+1}{[\cosh(p)+\cos(q)]^2},$$

where $p=(2d/\delta)(\sqrt{1+t^2}-t)^{1/2}$, $q=(2d/\delta)(\sqrt{1+t^2}+t)^{1/2}$, $t=\varepsilon\omega/\sigma$, and $\delta=\sqrt{2/\omega\sigma}$.

The real and imaginary parts of the Π flux are thus seen to correspond to the paramagnetic absorption (χ_A) and dispersion (χ_B), respectively [cf. Eqs. (11a) and (11b)]. For the EPR spectra analysis, only the ratio $P/Q=L$ is of importance.

From Eq. (15) it is clear that the EPR line shape in conducting media is subject to variation over wide limits. Because of this, the computer simulation of the EPR spectra was carried out by an optimization of the L_i, B_i, H_i^0, and ΔH_i parameters of the first derivatives of *N* Lorentzian lines of absorption and dispersion using the equation

$$\frac{dP}{dH} = \sum_{i=1}^{N}\frac{B_i}{\Delta H_i}\left[L_i\frac{1-x_i^2}{(1+x_i^2)^2} - \frac{2x_i}{(1+x_i^2)^2}\right], \tag{16}$$

where B_i is the amplitude of the *i*th absorption signal, ΔH_i is its linewidth, and $x_i=(H-H_i^0)/\Delta H_i$ with H_i^0 as the resonance field of the *i*th signal. It was found that the EPR spectra each of the investigated PAN-CSA_x and PAN-$AMPSA_x$ samples are fully described by Eq. (16) at $N=2$ with two signals R_1 and R_2 having different magnetic parameters and the degree of dispersion (L) depending on doping level, temperature, and size of the sample. Examples of the experimental and simulated EPR spectra at different temperatures are shown in Fig. 5. The detection of two EPR signals, R_1 and R_2, in the present study is in contrast with the previous report of only one Dysonian-like EPR line in the PAN-$AMPSA_{0.5}$ sample.[20]

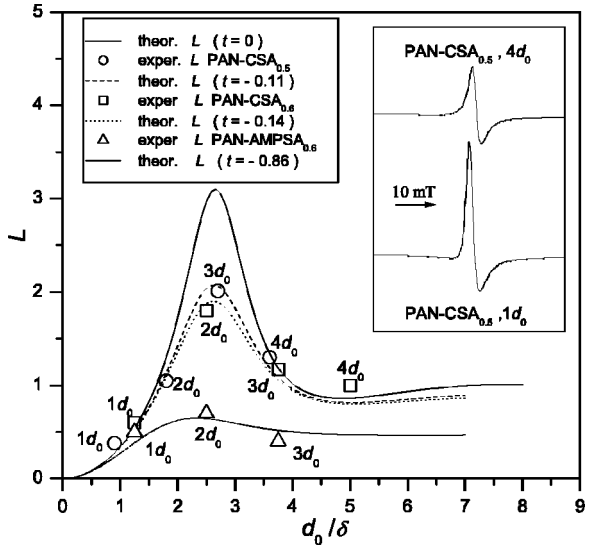

FIG. 6. The theoretical $L(d/\delta)$ dependences at different *t* values and experimental *L* magnitudes for the PAN-$CSA_{0.5}$, PAN-$CSA_{0.6}$, and PAN-$AMPSA_{0.5}$ films with different plate thicknesses (nd_0) at 9.3 GHz and 295 K. In the inset, the X-band EPR spectra of the PAN-$CSA_{0.5}$ films with the $1d_0$ and $4d_0$ thicknesses are shown.

For an analysis of the EPR line shape the analytical expression of the parameter $L=P/Q=L(d,\delta,t)$ is of interest. The calculated $L(d/\delta)$ dependences at different *t* values are shown in Fig. 6. From these plots it follows that the magnitude of *L* is sensitive to the change of both σ_{dc} and ε_{MW} values in a certain range of the d/δ ratio.

The way to test the calculated $L(d/\delta)$ dependences is to perform EPR experiments with samples having fixed skin depth δ and *t* (σ_{dc}=const, ε_{MW}=const) but different plate thickness, $2d$. This variation has been realized by gluing together films with the use of solvent, dichloroacetic acid. In these experiments, films of thickness d_0, $2d_0$, $3d_0$, and $4d_0$, with the starting film thickness $d_0=0.022$ mm for the PAN-$CSA_{0.5}$ film and $d_0=0.030$ mm for the PAN-$CSA_{0.6}$ and PAN-$AMPSA_{0.6}$ films (the condition $nd_0/\delta<5$ was satisfied) were used. The experimental data at 295 K and their approximated $L(d/\delta)$ dependences with *t* as a parameter of optimization are presented in Fig. 6. From so found values of the parameters $t=\varepsilon_{MW}\omega/\sigma_{dc}$ and $\delta=\sqrt{2/\omega\sigma_{dc}}$, the ε_{MW} and σ_{dc} values were estimated with an accuracy of the *L* and *d* determination errors.

As exemplified by Fig. 7, the σ_{dc} magnitudes measured directly and calculated from EPR data coincide within 5% for the PAN-$CSA_{0.5}$ and PAN-$CSA_{0.6}$ samples at different temperatures (above 10 K). For thin plates of PAN-$CSA_{0.5}$ and PAN-$AMPSA_{0.6}$ at $d_0/\delta<1$ the *t* parameter has little or no effect on the *L* value (Fig. 6) and hence an exact computation of σ_{dc} at one-film thickness is impossible. However, given the known σ_{dc} value at 295 K (Sec. III A), from the experimental *L* value at 295 K and calculated $L(d/\delta)$ dependence at $t=0$, the δ and d/δ parameters can be found at 295

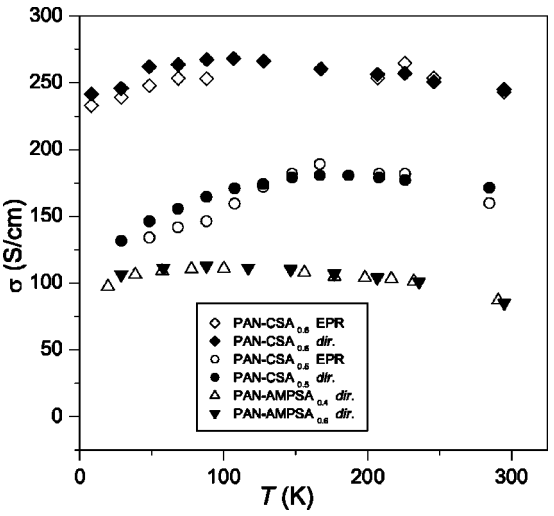

FIG. 7. A comparison between dc conductivities (σ_{dc}) measured directly and calculated from EPR data in the PAN-$CSA_{0.5}$ and PAN-$CSA_{0.6}$ samples at different temperatures.

K and then the d/δ and σ_{dc} values at different temperatures can be deduced from the experimental L magnitudes. The values obtained by this strategy for PAN-$CSA_{0.5}$ and PAN-$AMPSA_{0.6}$ films, as indicated in the lower inset at the right of Fig. 8, fit the theoretical $L(d/\delta)$ dependences for a t parameter falling in the broad range between 0 and -0.5. The $\sigma_{dc}(T)$ dependences calculated from this d/δ values for the PAN-$CSA_{0.5}$ and PAN-$AMPSA_{0.6}$ systems are in good agreement with corresponding $\sigma_{dc}(T)$ dependences obtained by direct conductivity measurements.

On the other hand, for thick plates ($d/\delta > 1$), from the known σ_{dc} at different temperatures the δ and d/δ parameters can be computed. From d/δ and the experimental L

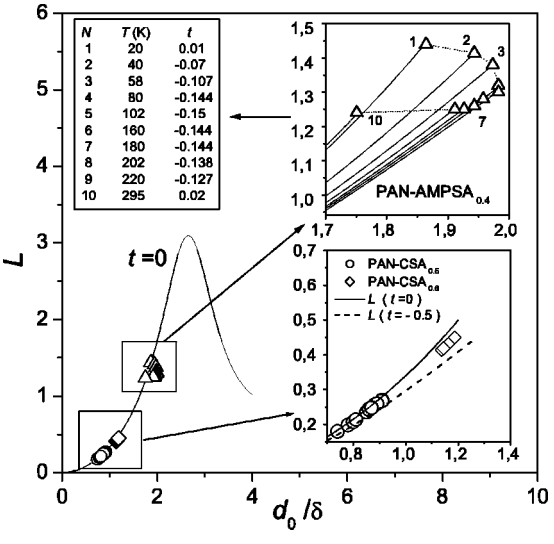

FIG. 8. The experimental L values at 9.3 GHz and calculated $L(d/\delta)$ dependences at different t magnitudes in the PAN-$CSA_{0.5}$ and PAN-$CSA_{0.6}$ films at 300 K (see the lower inset) as well as in the PAN-$AMPSA_{0.4}$ sample at different temperatures (see the upper inset and the table at the left of this inset).

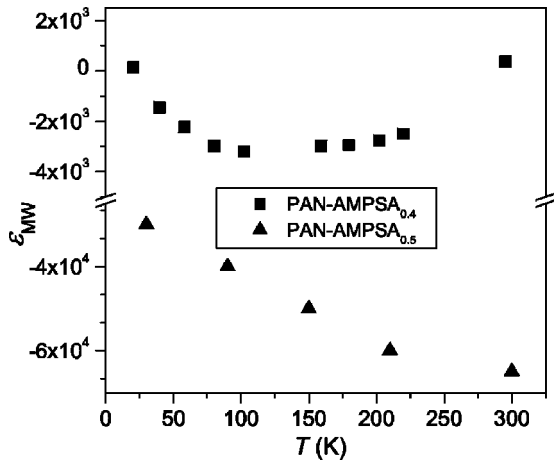

FIG. 9. The temperature dependence of the microwave dielectric constant (ε_{MW}) for the PAN-$AMPSA_{0.4}$ film at 9.3 GHz in comparison to that for the PAN-$AMPSA_{0.5}$ sample at 9.5 GHz from Ref. 20.

values, the t parameter for each temperature can be found graphically, as illustrated in the upper inset of Fig. 8 and in the table at the left of this inset. Using these t values the $\varepsilon(T) = t\sigma_{dc}/\omega$ dependence was calculated for the PAN-$AMPSA_{0.4}$ film (see Fig. 9). The relatively small ε magnitude ($|\varepsilon| < 10^3$) for this sample is evident from the EPR data at different frequencies, as presented in Fig. 10. Actually, with increasing frequency from 9.3 to 36.7 GHz the d/δ value doubles and the experimental L values corresponding to these frequencies lie exactly on the calculated $L(d/\delta)$ curve at $t = 0$. We point out that this result, along with our findings in experiments with variable film thicknesses (Fig. 6), strongly supports the validity of the calculated $L(d, \delta, t)$ dependence.

For both PAN-$CSA_{0.5}$ and PAN-$CSA_{0.6}$ films the calculated value of $\varepsilon_{MW} = t\sigma_{dc}/\omega$ averages to be about -5

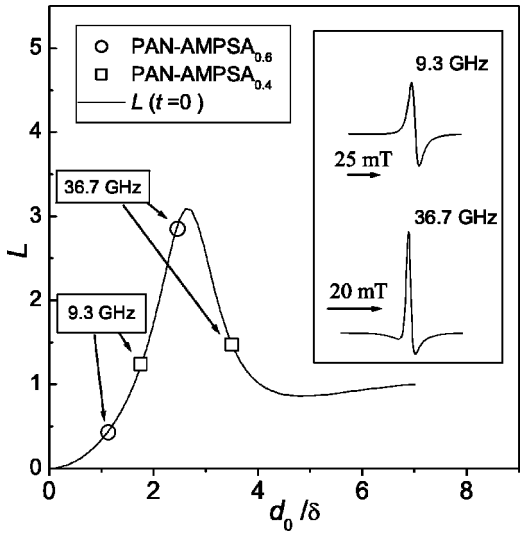

FIG. 10. The theoretical $L(d/\delta)$ dependence at $t = 0$ and experimental L values for the PAN-$AMPSA_{0.4}$ and PAN-$AMPSA_{0.6}$ samples at 9.3 and 36.7 GHz (300 K). In the inset the EPR spectra of the PAN-$AMPSA_{0.6}$ film at two frequencies are presented.

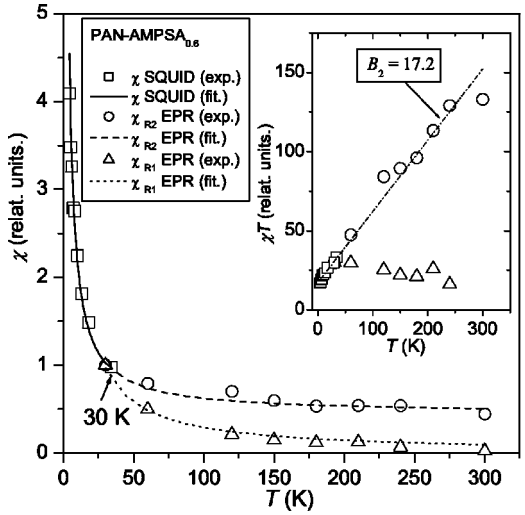

FIG. 11. The temperature dependences of the magnetic susceptibility (χ) and χT parameters (inset) for the R_1 and R_2 centers in the PAN-AMPSA$_{0.6}$ sample obtained by EPR and SQUID methods.

$\times 10^3$ at 300 K and 9.3 GHz and may be compared with the following reported data: $\varepsilon_{MW}=-4.4\times10^4$ at 300 K and 6.5 GHz for the best PAN-CSA$_{0.5}$ sample;[10] $\varepsilon_{MW}=-7\times10^4$ and -4×10^4 (300 K, 6.5 GHz) for the PAN-CSA$_{0.5}$ (*A*) and PAN-CSA$_{0.5}$ (*C*) samples, respectively;[13] and $\varepsilon_{MW}=-2\times10^2$ at 300 K and 100 GHz for PAN-CSA$_{0.5}$.[59] The deduced constant $\varepsilon_{MW}=-1.4\times10^4$ (300 K, 9.3 GHz) for the PAN-AMPSA$_{0.6}$ film is less than the published value $\varepsilon_{MW}=-6\times10^4$ (300 K, 9.5 GHz) for the PAN-AMPSA$_{0.5}$ sample.[20] In addition, the calculated $\varepsilon_{MW}(T)$ dependence for the PAN-AMPSA$_{0.4}$ film differs considerably from the $\varepsilon_{MW}(T)$ dependence obtained by a cavity perturbation method for the PAN-AMPSA$_{0.5}$ (see Fig. 9).[20] As temperature increases, the $\varepsilon_{MW}(T)$ parameter for PAN-AMPSA$_{0.4}$ passes through a minimum and approaches zero at 300 K (Fig. 9).

As is known,[10,12,13,20] the negative ε_{MW} values are evidence in favor of delocalized or metallic transport in the studied systems. The ε_{MW} increase at $T>200$ K for the PAN-AMPSA$_{0.4}$ sample suggests the localization of charge and correlates well with the high fraction of the DM phase (c_{DM}) in this film (Table II) and with a buildup of the DA phase at $T>240$ K, as mentioned above (Sec. III A).

C. EPR linewidth, magnetic susceptibility, and spin diffusion

As noted above, in the EPR spectra of the investigated systems two signals, R_1 and R_2, having different temperature dependences of intensity are observed. The intensity of the EPR signals was compared with the static magnetic susceptibility found from SQUID measurements. In view of the absence of a reliable standard for absolute susceptibility measurements with a *g*-factor differing essentially from 2.0023, only the relative susceptibilities derived by the two methods have been compared through the use of the χ normalization at $T=30$ K. As Fig. 11 suggests, the results of the χ measurements by the two methods are in close agreement. It was found that the R_1 signal susceptibility (χ_{R1}) obeys the Curie law, $\chi_{R1}=\chi_{C1}=B_1/T$, whereas the R_2 signal susceptibility (χ_{R2}) contains the Curie-like (χ_{C2}) and Pauli-like (χ_{P2}) contributions, $\chi_{R2}=\chi_{P2}+\chi_{C2}=A_2+B_2/T$. The obtained values of the normalized B_1, A_2, and B_2 parameters are listed in Table III and differ for the two methods by not more than 10%.

TABLE III. A comparison between the normalized magnetic-susceptibility parameters obtained from SQUID and EPR measurements for the PAN-AMPSA$_{0.4}$ and PAN-AMPSA$_{0.6}$ ($\chi_{R1}=\chi_{C1}=B_1/T$, $\chi_{R2}=\chi_{P2}+\chi_{C2}=A_2+B_2/T$).

	B_1 (K)		A_2		B_2 (K)	
Sample	SQUID	EPR	SQUID	EPR	SQUID	EPR
PAN-AMPSA$_{0.4}$		26	0.51	0.49	17.5	18.1
PAN-AMPSA$_{0.6}$		29	0.62	0.55	15.9	17.2

The fact that the χ_{R1} parameter obeys Curie's law proves the localized nature of the R_1 paramagnetic center, which can be assigned to the Ṅ-H radicals of isolated polymer chains. Actually, the EPR linewidth of the R_1 center (ΔH_{R1}) is essentially temperature independent, unlike the R_2 center linewidth, ΔH_{R2} (Figs. 12 and 13) and in good agreement with the rough estimation of the hyperfine interaction between the Ṅ-H electron and proton, $\Delta H_{R1}=\mu_e\mu_H/R^3\approx12$–15 G (at the Ṅ-H bond length $R\approx1$ Å).

On the other hand, the temperature dependence of χ_{R2} suggests that R_2 is an averaged signal resulted from exchange between localized and mobile spins with χ_{C2} and χ_{P2} susceptibilities respectively. The exchange is the reason why we do not observe an individual Dysonian line for the mobile (conduction) electrons ($L=P=Q=1$) but an averaged R_2 line with Lorentzian absorption and dispersion contributions [$L\neq1$, see Eq. (16)]. Introducing the constant of the spin equilibrium between conduction electrons (*e*) and localized spins (*s*), $K_{es}=\chi_{P2}/\chi_{C2}=A_2/B_2T^{-1}=C_2T$, from the

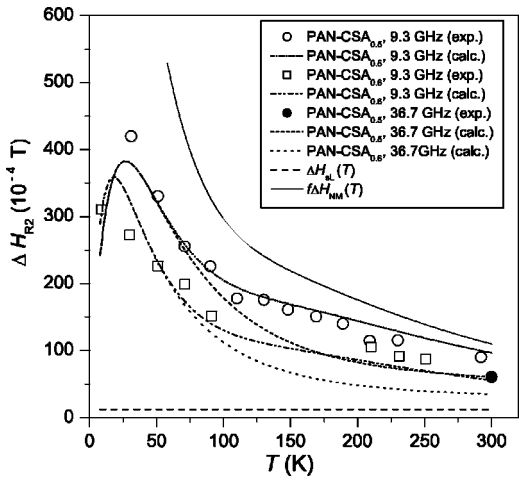

FIG. 12. The experimental (points) and calculated (lines) temperature dependences of the EPR linewidth (ΔH_{R2}) as well as the parameters ΔH_{sl} and $f\Delta H_{NM}$ [$f=c_{NM}/(c_{NM}+c_{DM})$] in the PAN-CSA$_{0.5}$ and PAN-CSA$_{0.6}$ films at 9.3 and 36.7 GHz.

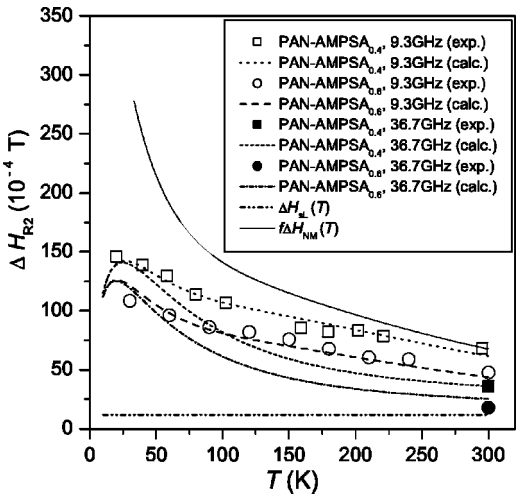

FIG. 13. The experimental (points) and calculated (lines) temperature dependences of the EPR linewidth (ΔH_{R2}) as well as the parameters ΔH_{sl} and $f\,\Delta H_{NM}$ $[f=c_{NM}/(c_{NM}+c_{DM})]$ in the PAN-AMPSA$_{0.4}$ and PAN-AMPS$_{0.6}$ samples at 9.3 and 36.7 GHz.

Bloch-Hasegava equations for rapid spin exchange in the bottleneck regime we have[60–62]

$$\Delta H_{R2}=\frac{\chi_{C2}}{\chi_{C2}+\chi_{P2}}\Delta H_{sl}+\frac{\chi_{P2}}{\chi_{C2}+\chi_{P2}}\Delta H_{el}$$
$$=\frac{1}{1+K_{es}}\Delta H_{sl}+\frac{K_{es}}{1+K_{es}}\Delta H_{el}, \qquad (17)$$

where ΔH_{R2} is the observed EPR linewidth and ΔH_{sl} and ΔH_{el} are the linewidths owing to the localized spin (s)-lattice (l) and mobile spin (e)-lattice (l) relaxations, respectively. In turn, the mobile electrons in the NM and DM phases can also be in the rapid spin-exchange state and by analogy with Eq. (17) in this case we get

$$\Delta H_{el}=\frac{c_{NM}}{c_{NM}+c_{DM}}\Delta H_{NM}+\frac{c_{DM}}{c_{NM}+c_{DM}}\Delta H_{DM}, \qquad (18)$$

where ΔH_{NM} and ΔH_{DM} are the EPR linewidths associated with intrinsic spin relaxation in the NM and DM phases, respectively, with the volume fractions of these phases, c_{NM} and c_{DM}, determined above (Sec. III A) from the conductivity measurements (Tables I and II).

It is apparent that the paramagnetic center with susceptibility χ_{C2} is located in the vicinity of mobile spins but this and the R_1 centers are the same in nature and hence $\Delta H_{R1}=\Delta H_{sl}\approx 12$ G. The transverse electron-spin relaxation rate (T_2^{-1}) for a dipole-dipole interaction between the mobile electron spins $S=1/2$ within the ''fast (f) motion'' region can be expressed by the relation[63]

$$T_{2f}^{-1}=\langle\Delta\omega^2\rangle[0.3\phi(0)+0.5\phi(\omega)+0.2\phi(2\omega)], \qquad (19)$$

where $\langle\Delta\omega^2\rangle=\gamma^4\hbar^2S(S+1)n\Sigma_{ij}$ is approximately the second moment of the internal field distribution with n being the electron-spin concentration per single monomer unit, Σ_{ij} the lattice sum for polycrystalline sample, $\phi(\omega)$ the motion spectrum, and ω the EPR frequency. In the full motion range from slow to the fast limit, the Eq. (19) is complicated and according to the previous suggestion[64] we finally obtain the following relation for T_2^{-1}:

$$\frac{1}{T_2}=\frac{\sqrt{3}}{2}\gamma\Delta H=\frac{1}{\langle\Delta\omega^2\rangle^{-1/2}+T_{2f}}. \qquad (20)$$

Unfortunately, it is almost impossible to estimate exactly the ΔH_{DM} values. However, one can justify the relation $\Delta H_{NM}\gg\Delta H_{DM}$ based on the following experimental facts (Figs. 12 and 13): (i) a marked frequency dependence of ΔH_{R2} occurs whilst the EPR linewidth in 3D metals is to be frequency independent, with the equality $T_1=T_2$ (T_1 and T_2 are the longitudinal and transverse spin-relaxation times);[65] (ii) the ΔH_{R2} reduction when passing from PAN-CSA$_{0.5}$ to PAN-CSA$_{0.6}$ and from PAN-AMPSA$_{0.4}$ to PAN-AMPSA$_{0.6}$ films correlates with decreasing NM phase fraction, $c_{NM}/c_{NM}+c_{DM}$ (see Tables I and II), and may be described with no regard for the ΔH_{DM} term in Eq. (19); (iii) assuming the spin-diffusion mechanism of the EPR linewidth narrowing for the DM phase from Eq. (19) with $n\approx 0.5$, $\Sigma_{ij}\approx 10^{57}$ m^{-6} (see Ref. 31), and correlation time τ_c as the reciprocal of the coefficient of spin diffusion ($D=\tau_c^{-1}$) lying in the D range from 5×10^{12} to 10^{15} rad/s at T between 10 and 300 K for the PAN-CSA$_x$ films,[50,51] we get the estimation of the value $\Delta H_{DM}=(2/\sqrt{3}\gamma)(1/T_2)$ of not more than 2 G, which is not in excess of the experimental error of the ΔH measurement. For the above reasons the assumption $\Delta H_{DM}=0$ can be taken.

We attempted to describe the experimental $\Delta H_{R2}(T)$ dependences in the context of the quasi-1D diffusion model for the NM phase with $\phi(\omega)$ given by Eq. (21),[66,67]

$$\phi(\omega)=\frac{1}{\sqrt{4D_{\parallel}D_{\perp}}}\left(\frac{1+\sqrt{1+(\omega/2D_{\perp})^2}}{1+(\omega/2D_{\perp})^2}\right)^{1/2}, \qquad (21)$$

where $D_{\parallel}$ and $D_{\perp}$ are the coefficients of spin diffusion along a polymer chain and between chains, respectively, with the latter corresponding to a cutoff frequency. However, Eqs. (17)–(21) with $\Delta H_{DM}=0$ give no satisfactory fit to the ΔH_{R2} frequency dependences (Figs. 12 and 13). Moreover, the $D_{\parallel}$ and $D_{\perp}$ values deduced from Eqs. (17)–(21) with the already mentioned n and Σ_{ij} magnitudes turn out to be closely related, $D_{\parallel}\approx D_{\perp}$, in contradiction with the quasi-1D diffusion hypothesis.

Such a result has forced us to use the 3D diffusion model for the NM phase with the ordinary motion spectrum,[63]

$$\phi(\omega)=\frac{2\tau_c}{1+\omega^2\tau_c^2}, \qquad (22)$$

involving of above-mentioned correlation time τ_c. As can be seen from Figs. 12 and 13, the experimental $\Delta H_{R2}(T,\omega)$ dependences in the PAN-CSA$_x$ and PAN-AMPSA$_x$ systems are well described by Eqs. (17)–(20) and (22) with the measured χ_{C2} and χ_{P2} values, the c_{NM} and c_{DM} magnitudes estimated from the conductivity data (Tables I and II), the assumption $\Delta H_{DM}=0$, and the calculated τ_c^{-1} vs temperature

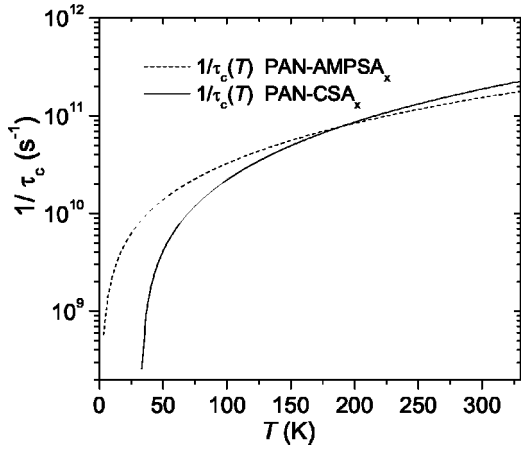

FIG. 14. The inverse correlation time τ_c^{-1} vs temperature dependences in the PAN-CSA$_x$ and PAN-AMPSA$_x$ systems calculated from the EPR data.

dependences are presented in Fig. 14. The enhanced ΔH_{R2} values for the PAN-CSA$_{0.5}$ and PAN-CSA$_{0.6}$ samples (Fig. 12) as compared to the PAN-AMPSA$_{0.4}$ and PAN-AMPSA$_{0.6}$ films (Fig. 13) can be assigned to the increased Σ_{ij} magnitude according to Eq. (19).

It is significant that each of the PAN-CSA$_x$ and PAN-AMPSA$_x$ systems was fitted with an unified $\tau_c^{-1}(T)$ dependence (Fig. 14) for all x values, thus strongly supporting our model. The calculated τ_c^{-1} temperature dependences in these systems differ markedly from the $D_{\|}(T)$ and $D_{\perp}(T)$ dependences derived in the PAN-CSA$_x$ or PAN-HCl$_x$ films by EPR data.[19,37,38] These discrepancies may be assigned to incorrect fitting of the EPR line shape in the previous works.

We point out the essential distinctions between the τ_c^{-1} and σ_{NM} temperature dependences for both studied systems. This is no surprise, since the conductivity σ_{NM} reflects mainly electron hopping between the metallic islands (Sec. III A) whereas the correlation time τ_c depends also upon the spin diffusion within these islands.

IV. CONCLUSIONS

We have advanced the multiphase heterogeneous granular metallic (HGM) effective-medium model taking into account disordered metallic (DM), nonmetallic (NM), and nonconducting (NC) phases. This model allowed us to describe quantitatively both charge transport and spin-diffusion phenomena in the doped polyaniline films, PAN-CSA$_x$ and PAN-AMPSA$_x$, in the full temperature range from 15 to 300 K with a unified set of parameters for all x values.

We have developed a method of analysis of the EPR line shape in conducting media. By this method conductivity and microwave dielectric constants for the polyaniline films were estimated from the EPR data. Two EPR signals, R_1 and R_2, have been detected in both systems and assigned to pinned and mobile paramagnetic centers, respectively. The temperature and frequency evolution of the R_2 signal is unambiguously explained in terms of three-site exchange between localized center and mobile spins in the NM and DM phases.

ACKNOWLEDGMENTS

The authors thank G. V. Mamin for recording of the EPR spectra and Yu. I. Talanov and N. N. Garif'yanov for taking of the SQUID measurements. This study was supported in part by the Russian Foundation for Basic Research (grant No. 01-03-33255) and the BRHE program (REC-007).

APPENDIX

Here we derive the relation (15) from the Eq. (14) [see Sec. III A]. In the conventional notations (SI system) the propagation constant k is written as $k=\alpha+i\beta$, defining $\alpha=\sqrt{\omega\sigma/2}\sqrt{\mu}(\sqrt{1+(\varepsilon\omega/\sigma)^2}-(\varepsilon\omega/\sigma))^{1/2}$ (fading coefficient) and $\beta=\sqrt{\omega\sigma/2}\sqrt{\mu}(\sqrt{1+(\varepsilon\omega/\sigma)^2}+(\varepsilon\omega/\sigma))^{1/2}$ (phase coefficient). We introduce for convenience the following notations:

$$kd=\tfrac{1}{2}\sqrt{\mu}(p+i\cdot q),$$

$$p=\frac{2d}{\delta}(\sqrt{1+t^2}-t)^{1/2},q=\frac{2d}{\delta}(\sqrt{1+t^2}+t)^{1/2},$$

with $t=\varepsilon\omega/\sigma$ and $\delta=\sqrt{2/\omega\sigma}$ being the skin depth. For paramagnetic material it is valid: $|\chi|\ll 1$, $\mu=1+\chi=1+(\chi'-i\chi'')$, and $\sqrt{\mu}=\sqrt{1+(\chi'-i\chi'')}\approx 1+1/2(\chi'-i\chi'')=1+\xi$ with $\xi=1/2(\chi'-i\chi'')$. The magnetic part of the flux of the complex Poynting vector per unit volume is

$$\Pi=\frac{2i\sqrt{\mu}\,\omega H_{mx0}^2}{(p+iq)}\tanh\left(\frac{\sqrt{\mu}}{2}(p+iq)\right),$$

or

$$\Pi\approx\frac{2i(1+\xi)\omega H_{mx0}^2}{(p+iq)}\tanh\left(\frac{(1+\xi)}{2}(p+iq)\right).$$

Expanding Π to a power series in ξ ($\xi\ll 1$) with an accuracy to the terms linear in ξ:

$$\Pi\propto P(\chi'-i\chi'')+Q(\chi''+i\chi')$$
$$=(P\chi'+Q\chi'')+i(Q\chi'-P\chi'')$$

with

$$P=\frac{1}{p^2+q^2}\frac{q\sinh(p)-p\sin(q)}{\cosh(p)+\cos(q)}+\frac{\sin(q)\sinh(p)}{[\cosh(p)+\cos(q)]^2},$$

$$Q=\frac{1}{p^2+q^2}\frac{p\sinh(p)+q\sin(q)}{\cosh(p)+\cos(q)}+\frac{\cos(q)\cosh(p)+1}{[\cosh(p)+\cos(q)]^2}.$$

*Electronic address: Valery.Shtyrlin@ksu.ru

[1] D.C. Trivedi, in *Handbook of Organic Conductive Molecules and Polymers*, edited by H.S. Nalwa (Wiley, Chichester, 1997), Vol. 2, pp. 505–571.
[2] N. F. Mott and E. Davis, *Electronic Processes in Non-Crystalline Materials* (Claredon Press, Oxford, 1979).
[3] N.F. Mott and M. Kaveh, Adv. Phys. **34**, 329 (1985).
[4] F. Zuo, M. Angelopoulos, A.G. MacDiarmid, and A.J. Epstein, Phys. Rev. B **36**, 3475 (1987).
[5] Z.H. Wang, A. Ray, A.G. MacDiarmid, and A.J. Epstein, Phys. Rev. B **43**, 4373 (1991).
[6] K. Lee, A.J. Heeger, and Y. Cao, Phys. Rev. B **48**, 14 884 (1993).
[7] Reghu Menon, C.O. Yoon, D. Moses, A.J. Heeger, and Y. Cao, Phys. Rev. B **48**, 17 685 (1993).
[8] Q. Li, L. Cruz, and P. Phillips, Phys. Rev. B **47**, 1840 (1993).
[9] R. Pelster, G. Nimtz, and B. Wessling, Phys. Rev. B **49**, 12 718 (1994).
[10] J. Joo, V.N. Prigodin, Y.G. Min, A.G. MacDiarmid, and A.J. Epstein, Phys. Rev. B **50**, 12 226 (1994).
[11] K. Lee, A.J. Heeger, and Y. Cao, Synth. Met. **72**, 25 (1995).
[12] R.S. Kohlman, J. Joo, Y.G. Min, A.G. MacDiarmid, and A.J. Epstein, Phys. Rev. Lett. **77**, 2766 (1996).
[13] R.S. Kohlman, A. Zibold, D.B. Tanner, G.G. Ihas, T. Ishiguro, Y.G. Min, A.G. MacDiarmid, and A.J. Epstein, Phys. Rev. Lett. **78**, 3915 (1997).
[14] J. Joo, S.M. Long, J.P. Pouget, E.J. Oh, A.G. MacDiarmid, and A.J. Epstein, Phys. Rev. B **57**, 9567 (1998).
[15] P. Rannou, M. Nechtschein, J.-P. Travers, D. Berner, A. Wolter, and D. Djurado, Synth. Met. **101**, 734 (1999).
[16] E.P. Nakhmedov, V.N. Prigodin, and A.N. Samukhin, Sov. Phys. Solid State **31**, 368 (1989).
[17] R. Mennon, C.O. Yoon, D. Moses, and A.J. Heeger, in *Handbook of Organic Conductive Molecules and Polymers*, edited by H.S. Nalwa (Wiley, New York, 1996).
[18] Z.H. Wang, E.M. Scherr, A.G. MacDiarmid, and A.J. Epstein, Phys. Rev. B **45**, 4190 (1992).
[19] V.I. Krinichnyi, S.D. Chemerisov, and Y.S. Lebedev, Phys. Rev. B **55**, 16 233 (1997).
[20] W.-P. Lee, K.R. Brenneman, A.D. Gudmundsdorttir, M.S. Kahol, A.P. Monkman, and A.J. Epstein, Synth. Met. **101**, 819 (1999).
[21] V.N. Prigodin, Synth. Met. **84**, 705 (1997).
[22] A.N. Samukhin, V.N. Prigodin, L. Jastrabik, and A.J. Epstein, Phys. Rev. B **58**, 11 354 (1998).
[23] P. Sheng, B. Abeles, and Y. Arie, Phys. Rev. Lett. **31**, 44 (1973).
[24] B. Abeles, P. Sheng, M.D. Coutts, and Y. Arie, Adv. Phys. **24**, 407 (1975).
[25] C.J. Adkins, J. Phys. C **20**, 235 (1987); **15**, 7143 (1982).
[26] A.B. Kaiser, C.K. Subramaniam, P.W. Gilberd, and B. Wessling, Synth. Met. **69**, 197 (1995).
[27] B. Sixou, J.-P. Travers, and Y.F. Nicolau, Synth. Met. **84**, 703 (1997).
[28] E.R. Holland, S.J. Pomfret, P.N. Adams, and A.P. Monkman, J. Phys.: Condens. Matter **8**, 2991 (1996).
[29] P.N. Adams, P. Devasagayam, S.J. Pomfret, L. Abell, and A.P. Monkman, J. Phys.: Condens. Matter **10**, 8293 (1998).
[30] P. Sheng, Phys. Rev. B **21**, 2180 (1980).
[31] V.I. Krinichnyi, Russ. Chem. Rev. **65**, 521 (1996).
[32] V.I. Krinichnyi, I.B. Nazarova, L.M. Goldenberg, and H.-K. Roth, Polym. Sci., Ser. A Ser. B **40**, 835 (1998).
[33] A.P. Monkman, D. Bloor, and G.C. Stevens, J. Phys. D **23**, 627 (1990).
[34] M. Iida and T. Asaji, Synth. Met. **55-57**, 607 (1993).
[35] K. Mizoguchi, M. Nechtschein, J.-P. Travers, and C. Menardo, Phys. Rev. Lett. **63**, 66 (1989).
[36] K. Mizoguchi, M. Nechtschein, and J.-P. Travers, Synth. Met. **41-43**, 113 (1991).
[37] K. Mizoguchi and K. Kume, Synth. Met. **69**, 241 (1995).
[38] M.C. Itow, T. Kawahara, N. Kachi, H. Sakkamoto, K. Mizoguchi, K. Kume, Y. Sahara, S. Masubuchi, and S. Kazama, Synth. Met. **84**, 749 (1997).
[39] K.R. Brenneman, J. Feng, Y. Zhou, A.G. MacDiarmid, M.S. Kahol, and A.J. Epstein, Synth. Met. **101**, 785 (1999).
[40] M.S. Kahol, Solid State Commun. **117**, 37 (2001).
[41] P.N. Adams, P.J. Laughlin, A.P. Monkman, and A.M. Kenwright, Polymer **37**, 3411 (1996).
[42] A.L. Efros and B.I. Shklovskii, J. Phys. C **8**, L49 (1975).
[43] B.I. Shklovskii and A.L. Efros, *Electronic Properties of Doped Semiconductors* (Springer-Verlag, New York, 1984).
[44] L. Zuppiroli, M.N. Bussac, S. Paschen, O. Chauvet, and L. Forro, Phys. Rev. B **50**, 5196 (1994).
[45] M. Kaveh and N.F. Mott, J. Phys. C **15**, L707 (1982).
[46] K.F. Berggren, J. Phys. C **15**, L45 (1982).
[47] M. Kaveh and N.F. Mott, J. Phys. C **15**, L697 (1982).
[48] P.A. Lee and T.V. Ramakrishnan, Rev. Mod. Phys. **57**, 287 (1985).
[49] A.G. Zabrodskii, S.A. Nemov, and Y.I. Ravich, *Electronic Properties of Disordered Systems* (Nauka, St. Petersburg, 2000).
[50] B. Beau, J.-P. Travers, and E. Banka, Synth. Met. **101**, 772 (1999).
[51] B. Beau, J.-P. Travers, F. Genoud, and P. Rannou, Synth. Met. **101**, 778 (1999).
[52] M. Jonson and S.M. Girvin, Phys. Rev. Lett. **43**, 1447 (1979).
[53] S.M. Girvin and M. Jonson, Phys. Rev. B **22**, 3583 (1980).
[54] D. Belitz and W. Gotze, J. Phys. C **15**, 981 (1982).
[55] D. Belitz and W. Schrimacher, J. Phys. C **16**, 913 (1983).
[56] F. Leclerq and P. Damay, Philos. Mag. B **57**, 61 (1988).
[57] T.S. Altshuler, O.B. Vinogradova, A.F. Kukovizkii, and E.G. Kharakhashjan, Fiz. Tverd. Tela (Leningrad) **15**, 3602 (1973).
[58] F.J. Dyson, Phys. Rev. **98**, 349 (1955).
[59] H.C.F. Martens, H.B. Brom, J.A. Reedijk, and de D.M. Leeuw, Synth. Met. **101**, 821 (1999).
[60] S.E. Barnes, Adv. Phys. **30**, 801 (1981).
[61] L.R. Tagirov and K.F. Trutnev, Sov. Phys. JETP **59**, 638 (1984).
[62] V.A. Atsarkin and V.V. Demidov, Sov. Phys. JETP **86**, 572 (1998).
[63] A. Abragam, *The Principles of Nuclear Magnetism* (Oxford University Press, Oxford, 1961).
[64] V.A. Atsarkin, V.V. Demidov, and G.A. Vasneva, Phys. Rev. B **56**, 9448 (1997).
[65] V.V. Andreev and V.I. Gerasimenko, Zh. Eksp. Teor. Fiz. **35**, 1209 (1958).
[66] G. Soda, D. Jerome, M. Weger, J. Alizon, J. Gallice, H. Robert, J.M. Fabre, and L. Giral, J. Phys. (France) **38**, 931 (1977).
[67] C. Jeandey, J.P. Boucher, F. Ferrieu, and M. Nechtshein, Solid State Commun. **23**, 673 (1977).